J Polym Res (2015) 22: 42
DOI 10.1007/s10965-015-0688-4

ORIGINAL PAPER

Enhancement in pyroelectric detection sensitivity for flexible $LiNbO_3$/PVDF nanocomposite films by inclusion content control

M. S. Jayalakshmy · J. Philip

Received: 9 October 2014 / Accepted: 23 February 2015 / Published online: 1 March 2015

Abstract The pyroelectric properties of polymer-ceramic nanocomposites of Lithium niobate/Poly (vinylidene fluoride) or $LiNbO_3$/PVDF (abbreviated LN/PVDF) for thermal/infrared sensing applications are reported in this work. The composites are prepared by dispersing nanoparticles of $LiNbO_3$, with particle size in the range 45–65nm, in β-PVDF matrix at varying volume fractions, and cast in the form of flexible films by solvent-cast technique. The electro-active β-phase of PVDF is confirmed by powder X-ray Diffraction (XRD), Fourier Transform Infrared Spectroscopy (FT-IR) and Differential Scanning Calorimetry (DSC) analyses. The thermal properties, thermal conductivity and specific heat capacity, of the composites are determined by a photothermal technique. The prepared films have been poled in a high *dc* electric field, and their pyroelectric and dielectric properties measured by direct methods. From these data the pyroelectric figures of merit of the composite films have been determined and their values compared with corresponding values for pure PVDF film. The Shore hardness of the films has been measured to estimate the extent to which the flexibility of the films is affected by the addition of ceramic. Significant enhancement in pyroelectric sensitivity has been obtained with increase in volume fraction of $LiNbO_3$ nanoparticles. However, this enhancement is at the expense of the flexibility of the composite; so one has to strike a balance between the two while selecting a suitable composition for the development of pyroelectric sensors with these materials. The results of this work provide guidelines for this selection.

Keywords Lithium niobate · Poly (vinylidene difluoride) · Nanocomposites · Pyroelectricity · Pyroelectric figure of merit · Photothermal technique

M. S. Jayalakshmy · J. Philip
Department of Instrumentation, Cochin University of Science and Technology, Cochin 682 022, India

M. S. Jayalakshmy
e-mail: jayalakshmy.ms@gmail.com

J. Philip (✉)
Amal Jyothi College of Engineering, Kanjirappally, Kottayam 686518, India
e-mail: jphilip6012@gmail.com

Introduction

Even though many of the remarkable electrical properties of pyroelectric materials have been known for years, surprising new effects and practical applications are being discovered with advent of materials in their nanoforms [1–6]. Among many fundamental properties of nanomaterials, the pyroelectric properties are being exploited for technological applications ranging from basic sensing and detection to security systems. Pyroelectric materials take the most important role as pyroelectric infrared detectors [7–9]. Under equilibrium conditions the bound polarization charges at the surface of a pyroelectric material are screened by (mobile) compensation charges [10]. A temperature change results in a change in the magnitude of polarization leading temporarily to an imbalance between bound polarization charges and the remaining screening charges at the surface [11]. This effect is employed in various thermal and infrared detectors whereby the pyroelectric potential is converted into a current signal through the electrical contacts at opposite surfaces of the pyroelectric element [12, 13]. Pyroelectric single crystals, ferroelectric ceramic materials as well as electro-active polymers have been used since the 1960s for thermal and infrared (IR) detection applications [13–15]. A variety of materials used for this application can be found in literature [15].

Thermal detectors measure IR radiation indirectly by measuring the temperature change due to absorption of radiation. They are widely used for contactless temperature measurement, security detectors (intruder alarms), human presence sensors and thermal imaging. Although mostly promoted by military interest in night time warfare, low-cost IR imaging techniques based on pyroelectric detectors also have a number of industrial, medical and other civil applications where useful information is obtained by detecting IR radiation [15–18]. Sensor systems based on pyroelectric ceramic/polymer composites have acquired popularity for the following reasons; light weight, immunity to corrosion, performance over wide temperature range, physical flexibility, mouldability and higher sensitivity as compared to existing sensor materials. A good amount of work has already appeared in literature on the preparation and properties of such composites [19]. However, commercial detectors based on them have not yet appeared in the market.

A survey of literature on polymer-ceramic composites for sensor applications reveal that most of the work in this area have been on composites prepared by mixing the polycrystalline ceramic with an electro-active polymer. Such composites have many of the shortcomings of the parent ceramic, like high hardness and brittleness; at the same time less sensitivity due to large volume of the material occupied by the polymer matrix. However, if the ceramic is prepared in the nanocrystalline form, with particle sizes typically less than 100 nm, one can develop polymer-ceramic nanocomposites with better sensitivity, though not as high as the original ceramic. At the same time, such a composite has all the desirable properties of the polymer matrix, such as flexibility, robustness and possibility to cast in the form of thin sheets or even films. Moreover, since the inclusions have particle sizes in the nanometer range, one can hope to achieve higher sensitivity at lower concentrations of the ceramic, compared to the corresponding polymer- polycrystalline ceramic. It is known that ferroelectricity (or pyroelectricity) in a ceramic vanishes when particle sizes are reduced to nanometer scales. However, this happens only when particle sizes are below typically 20–10 nm, depending on the material. It is only recently that scientists developed techniques to prepare pyroelectric ceramics in the nanocrystalline form with control over particle sizes. So serious work on the development of such smart materials has begun only recently, and commercial sensors based on them are likely to appear shortly.

In this work, investigations have been carried out on the development of LN/PVDF nanocomposites with high enough pyroelectric figures of merit and low enough mechanical hardness to keep the material flexible so that mouldable thermal and infrared detectors can be developed for commercial applications.

$LiNbO_3$ (LN) is a well known ferroelectric material with very wide technological applications for its interesting physical properties like birefringence, high piezoelectricity, pyroelectricity, and acousto-optic, electro-optic as well as photo-elastic coefficients [20–23]. Compared to other commonly used pyroelectrics like Triglycine sulfate, Barium titanate, or Lead-based titanates or germanates, the rare combination of several material properties and technological advantages make LN the most favoured material for a variety of applications in technology. The material can be prepared in the laboratory without much difficulty, it is non-toxic, insoluble in water, and its polarization is highly stable even in unidirectional poled material at nanometer scales. LN is a naturally stable material because it has no phase transition below its high Curie temperature (1200 °C) [24]. At room temperature it has a rhombohedral symmetry with space group $R3c$.

PVDF is a semi-crystalline polymer with at least four crystalline phases [25, 26]. These phases include the nonpolar α-phase, polar β and γ phases and the δ phase. Only the β-phase exhibits the pyro, piezo, dielectric and related properties. An easy method to obtain the β-crystalline phase of PVDF films is mechanical stretching. Also, use of certain solvents like Dimethyl sulfoxide (DMSO), Dimethylformamide (DMF) etc. results in β-phase PVDF films after casting. The β-phase PVDF is currently available commercially as thermal and strain sensors which respectively employ the pyroelectric and piezoelectric properties of this material. Being a representative ferroelectric electro-active polymer with inherently high pyroelectric and piezoelectric properties and with high dynamic response for use in touch/tactile sensors, infrared detectors and vidicon/imaging devices, Poly (vinylidene fluoride) or PVDF is selected as the host polymer in this work [27, 28]. Nowadays, high efficiency becomes a prerequisite in many application fields such as sensors, information storage, etc. To meet this end it is very easy to prepare thin films of PVDF containing high content of β-phase. This is also a reason for selecting PVDF as the polymer matrix in this work.

As polymers possess high strength, good flexibility, easy processing, and low cost, combining LN with polymers like PVDF would be promising for the development of sensor materials [29]. The present work aims at the preparation of ceramic/polymer nanocomposites of LN/PVDF by dispersing nanoparticles of LN in PVDF, with varying concentrations of LN, and measuring their structural, dielectric, thermal, mechanical and pyroelectric properties, and estimating their pyroelectric figures of merit. The objective of preparing LN as nanoparticles is to attain better flexibility without compromising on the detection sensitivity for lower concentrations of the ceramic. Procedures followed to prepare the samples and experimental methods employed to study their properties are outlined below. Results of these investigations as well as the pyroelectric figures of merit of the prepared compositions are presented and discussed in the following sections.

Experimental

Materials

In order to prepare LN nanoparticles, analytically pure Nb_2O_5 (99.999 %, Sigma Aldrich), Hydrofluoric acid (HF) (40 % *v*/*v*), standard Ammonia (25 % *v*/*v*), Ammonium oxalate (99.99 % *w*/*w*, Sigma Aldrich) and Li (OH) (Sigma Aldrich) were used as the starting materials. The polymer matrix used in this study was commercially available PVDF (Sigma Aldrich) with average molecular weight ~534,000. In order that the β-phase of PVDF was formed upon casting to solid, the polymer was dissolved in DMF.

Methods

LN nanoparticles were prepared following a chemical route. Stoichiometric amount of Nb_2O_5 was dissolved in minimum amount of HF after heating in a hot water bath at 98 °C for 20 h. The ratio of Nb_2O_5 to HF was taken as one. It was then mixed with 1.2 mol/l Ammonium oxalate solution by keeping the ratio Ammonium oxalate: Nb_2O_5 (V/W)=5 l: 1.5 mol. During addition of Ammonia solution $Nb(OH)_5$ began to precipitate. This precipitate was washed several times with dilute Ammonia solution and plenty of hot water. This filtered cake was then dried in an oven at about 65 °C for 2 h. Then the two hydroxides Li(OH) and $Nb(OH)_5$ were taken in stoichiometric ratio and mixed, ground well several times in an agate mortar using acetone as grinding medium for 2 h. Finally the mixture was heated at 850 °C for 4 h. Powder XRD (Make: Bruker, Model: AXS D8 Advance) was employed to characterize the prepared powder. XRD patterns were recorded for LN nanoparticles sintered at various temperatures.

A solvent cast technique was adopted for fabricating films of pure PVDF as well as LN/PVDF nanocomposites [30]. In order to investigate the variations in properties of the composites with concentration of LN, different volume fractions of LN (0.001, 0.01, 0.05, 0.09, 0.15 and 0.25) were dispersed in PVDF matrix so as to synthesize LN/PVDF nanocomposites. A sample of pure PVDF film was also synthesized for comparison with the composites. The pure PVDF film was also characterized using XRD, FT-IR (Make: Thermo Nicolet, Model: Avatar 370) and DSC (Make: Mettler Toledo, Model: DSC 822^e) to confirm the β-phase of PVDF. Films with volume fraction only up to 0.25 of LN could be fabricated due to problems of particle agglomeration and nonuniformity at higher inclusion concentrations.

For dielectric and pyroelectric measurements small pieces of dry composite samples were coated with a thin layer of silver paste The dielectric constant (ε') and dielectric loss (ε') of the samples were measured with an Impedance analyzer (Make: Hioki, Model: IM 3570) in the frequency range 100 Hz–5 MHz.

The pyroelectric coefficients *p(T)* of the nanocomposite films were measured by the Byer and Roundy method [31]. This method is a more straight forward one than the dynamic or charge integration technique. The working principle of thermal/pyroelectric IR detectors is that the absorbed heat energy results in a corresponding increase in temperature *(dT)* and spontaneous polarization of the material. Changes in polarization alter the surface charge of the electrodes and to keep neutrality charges are expelled from the surface which results in a pyroelectric current in an external circuit. The pyroelectric current depends on the temperature change with time. The pyroelectric current I is proportional to the electrode area A of the sample and the rate of change of temperature *(dT/dt),* from which the pyroelectric coefficient can be obtained as

$$p(T) = \frac{I}{A} \times \frac{1}{dT/dt} \tag{1}$$

In all our measurements the sample heating rate was kept at 2 °C/min.

The pyroelectric properties of PVDF and its co-polymers can be enhanced by poling. Poling is a process of converting a multi-domain single crystal to a single domain one with application of an external electric field far greater than the coercive field in the direction of polarization axis. The PVDF material can retain its pyroelectric properties only up to a certain value of the electric field. Beyond this it gets depoled (loses its pyroelectric/piezoelectric properties). Poling can be done either by contact poling, where the electric field is directly applied across the film through two contact electrodes, or by corona poling, in which the film has an electrode fixed only to one side and a sharp needle placed at a certain distance away from the other side. When a very high voltage is applied across the needle and the bottom electrode, ionization of air occurs around the needle and the generated charges get accumulated on the film surface establishing a poling electric field in the film [32, 33]. In the present investigations we have adopted the corona technique for poling the samples. All the samples in circular shape having diameter 4 cm were uniformly poled by a single corona point under a field of 23 MV/m at 80 °C for 1 h.

Thermal properties of LN/PVDF nanocomposites were measured following a photothermal technique, with a pyroelectric detector used as the thermal detector [34]. The basic principle of the technique is that, when a periodically modulated light beam from a light source impinges on the surface of the sample, the sample absorbs part of the incident energy. The sample undergoes a non-radiative de-excitation process and gets correspondingly heated. This periodic temperature variation in the sample can be directly detected with a sensitive pyroelectric transducer kept in intimate contact with the

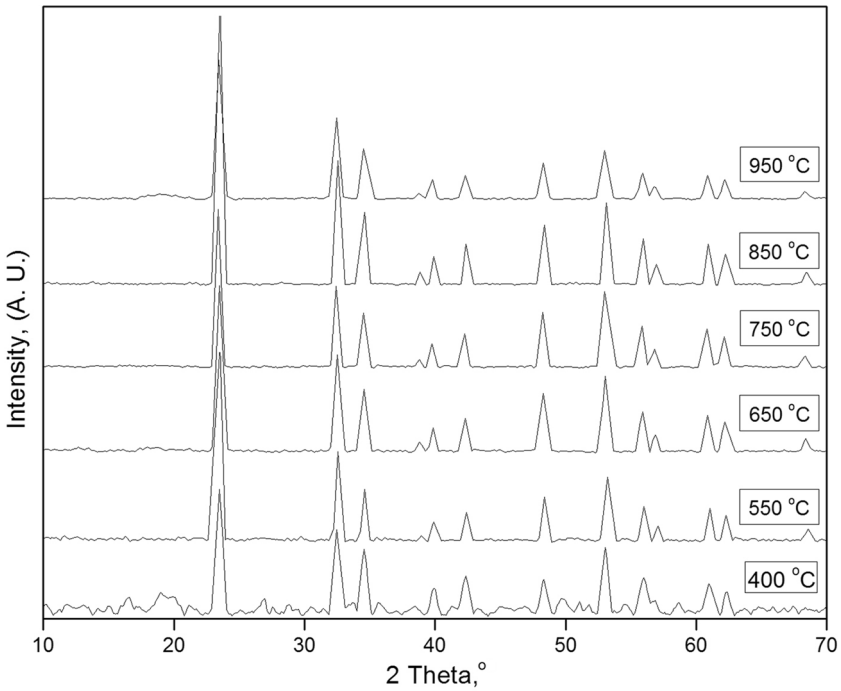

Fig. 1 X-ray diffraction patterns of LN nanopowders sintered at different temperatures (Step size: 0.020°, Step time: 31.2 s)

sample. In the present work, a 120 mW He-Cd laser of wavelength 442 *nm*, intensity modulated by a mechanical chopper, was used as the optical heating source. A nickel-chromium coated PVDF film of thickness 28 μm, and pyroelectric coefficient 30 $\mu Cm^{-2}\ K^{-1}$was used as the pyroelectric detector. The sample-detector assembly was mounted on a thermally thick backing. The modulation frequency of light was kept above 60 Hz to ensure that the detector, the sample and the backing were thermally thick during measurements. The output signal was measured with a dual-phase lock-in amplifier (Make: Stanford Research Systems, Model: SR830). Measurement of amplitude and phase of the output signal enabled us to determine the thermal diffusivity *(α)* and thermal effusivity *(e)*, from which the thermal conductivity *(k)* and volume specific heat capacity *(C)* of the sample could be obtained.

The Shore D hardness values for the samples, including pure PVDF, were measured following indentation method,

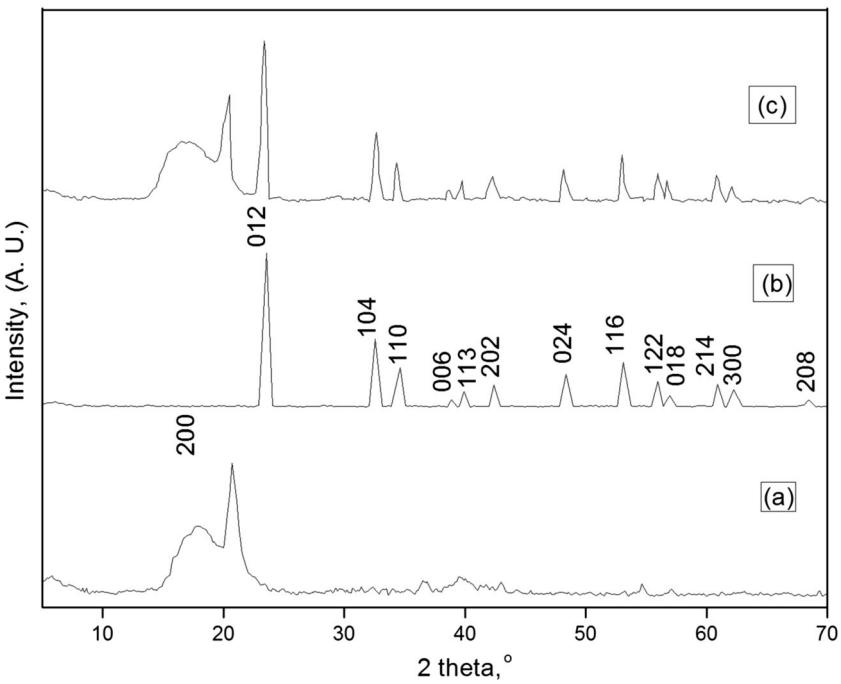

Fig. 2 X-ray diffraction pattern of (**a**) pure PVDF film, (**b**) LN nanopowder, (**c**) LN/PVDF nanocomposite with volume fraction 0.05 of LN (Step size: 0.020°, Step time: 31.2 s)

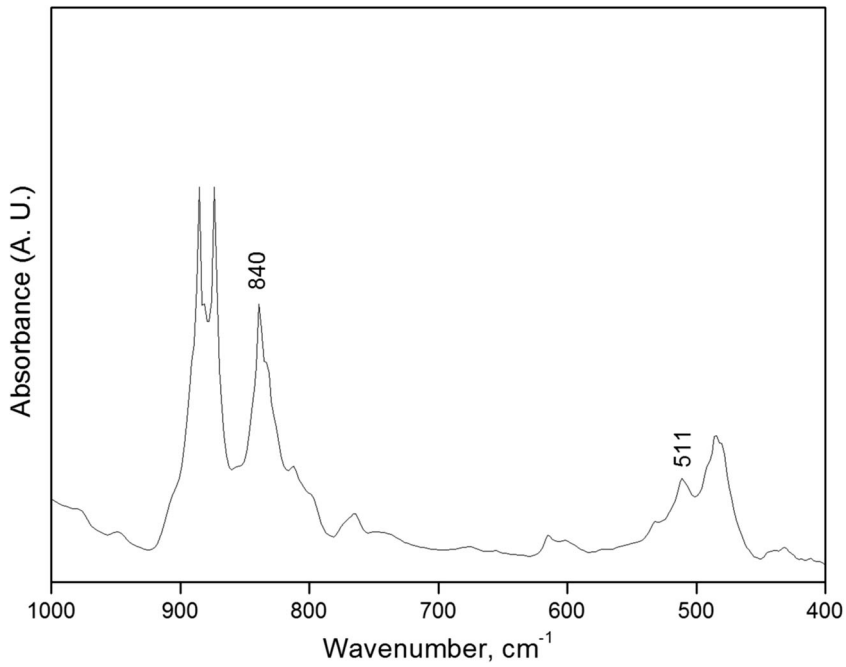

Fig. 3 FTIR spectrum of pure PVDF film

measuring the penetration depth of a durometer indenter with a Shore hardness meter (Make: Hardmatic Mitutoyo, Model: 321JAA283).

Characterization

The powder XRD patterns for the LN nanoparticles sintered at different temperatures are shown in Fig. 1. The powder XRD pattern of pure PVDF sample (Fig. 2a) shows a major peak at 20.5° (corresponding to the (200) plane), which is the prominent peak for the β-phase of PVDF [35]. The FT-IR spectrum of pure PVDF sample is shown in Fig. 3. Here the absorption peaks at 511 and 840 cm^{-1} are the characteristic ones for β--PVDF [35, 36]. From the figure it is clear that the characteristic peaks corresponding to α-phase (766, 795, 856 and 976 cm^{-1}) and γ-phase (778, 812 and 834 cm^{-1}) of PVDF are absent in the FT-IR spectrum [36]. This shows that PVDF formed is predominantly β-phase. From the DSC curve

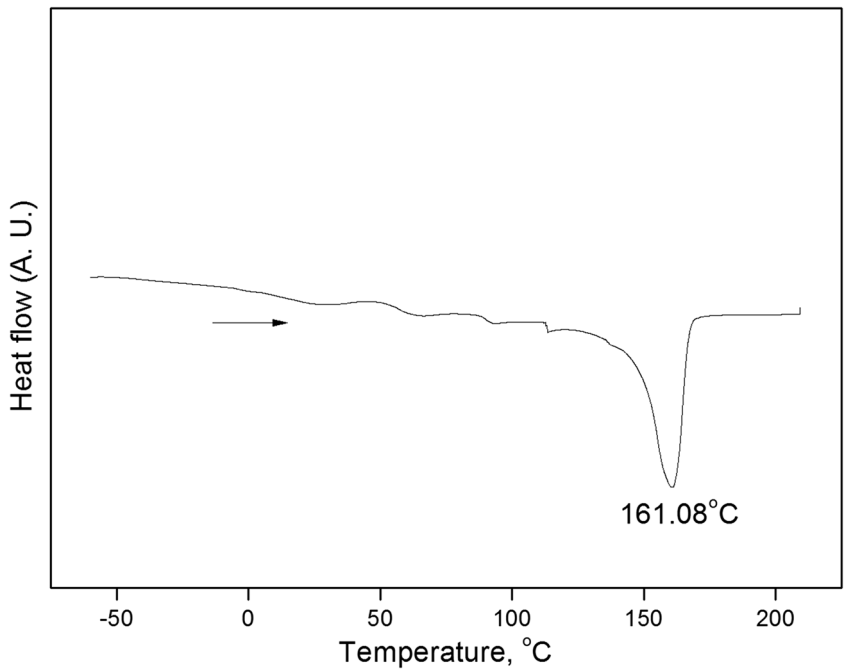

Fig. 4 DSC curve of pure PVDF film during heating cycle (Heating rate 10 °C/min)

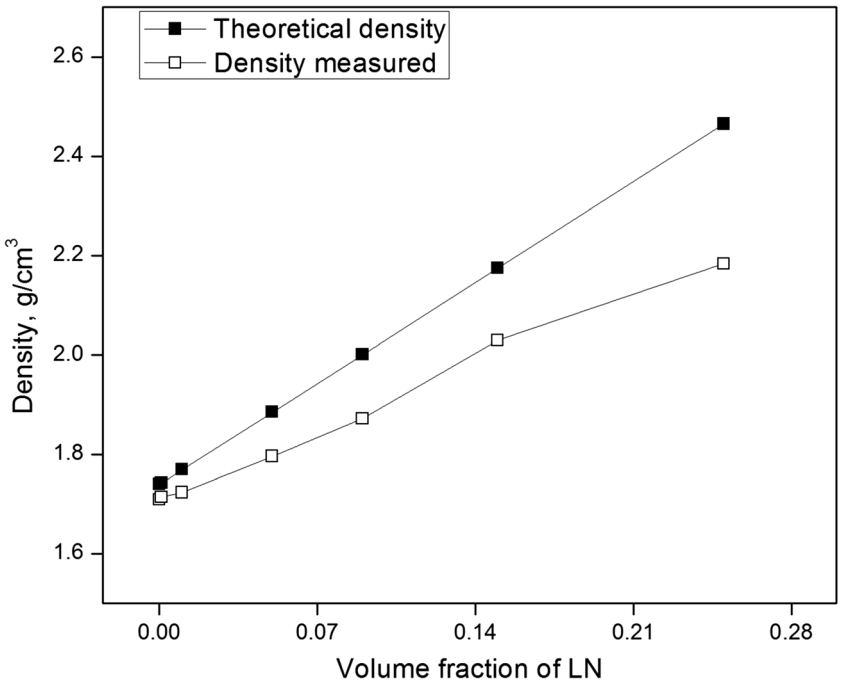

Fig. 5 Variations of theoretical and experimental densities of LN/PVDF nanocomposites with varying volume fractions of LN

(Fig. 4) it is found that the melting point of the PVDF film cast from DMF solvent is 161.18 °C. No other transition peak is found in the temperature region of the measurements.

The X-ray powder diffraction patterns of the newly prepared samples show only the reflection peaks of the hexagonal $LiNbO_3$ structure. All the *d*-line patterns match with reported values (JCPDS-20-631) (Fig. 2b). As can be seen in Fig. 1, the beginning of crystallization can be detected starting from 400 °C, and at 650 °C all reflections are observed. The intensity of the reflections increases with increasing sintering temperature which indicates a higher degree of crystallinity for the material and maximum observed at 850 °C. The average particle size obtained using the Debye - Scherrer formula is in the range 45–65 nm.

Each of the LN/PVDF nanocomposite films has also been subjected to powder XRD measurements. The XRD pattern for one LN/PVDF composite sample (with volume fraction 0.05) is also shown in Fig. 2c. Peaks in the XRD pattern for this sample confirm the presence of LN nanoparticles in PVDF matrix.

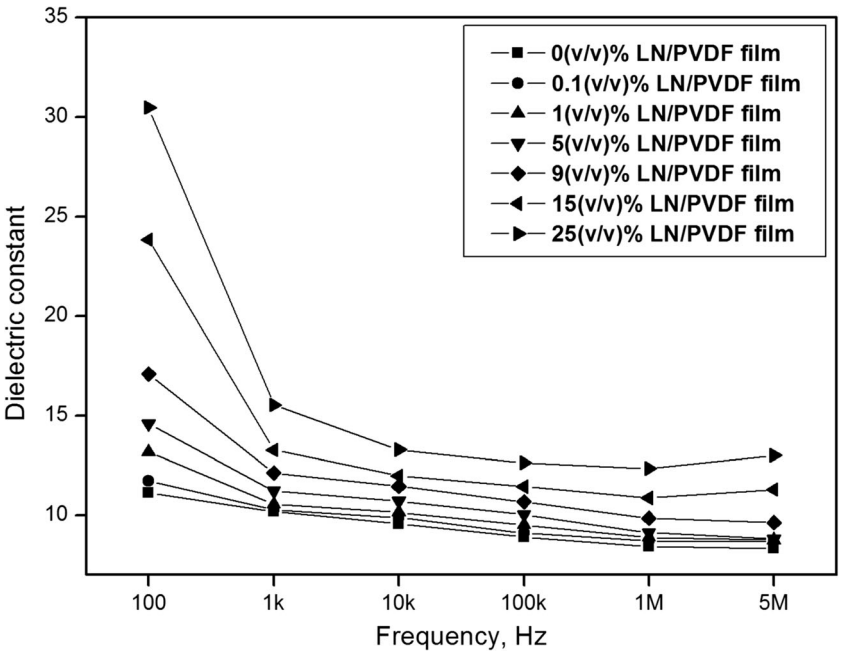

Fig. 6 Variations of dielectric constant with frequency for different LN/PVDF nanocomposites

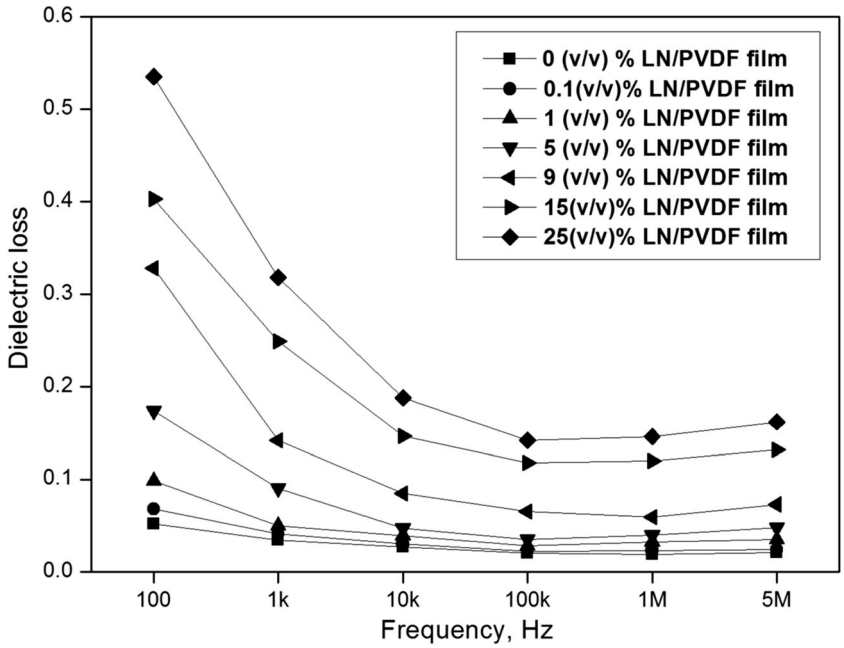

Fig. 7 Variations of dielectric loss with frequency for different LN/PVDF nanocomposites

Results and discussion

A comparison of the theoretical and experimental densities of the composites with varying volume fractions of LN are shown in Fig. 5. Theoretical densities of the composites are calculated following the rule of mixtures. Densities have also been measured directly. It can be inferred that the density increases with filler concentration, and it is slightly lower than the theoretical density in all cases. This could be due to the possible presence of voids and defects in the composites during preparation. At high filler loadings, certainly there is a possibility for the ceramic particles to form aggregates, which may tend to settle. This may cause nonuniformity in the density of the samples, reducing the density in the upper regions of the cast films. However, all of the prepared samples have attained a density in the range 95–90 % of the theoretical density as the filler volume fraction increases from 0 to 0.25.

Variations of dielectric constant and dielectric loss with frequency for samples with different concentrations of nano LN in PVDF are shown in Figs. 6 and 7. It can be seen that both dielectric constant and loss increase at all frequencies as the LN content in the matrix increases. Dielectric constant varies from 10.19 to 15.53 as the volume fraction of LN increases from 0 to 0.25 at 1 kHz, whereas the corresponding

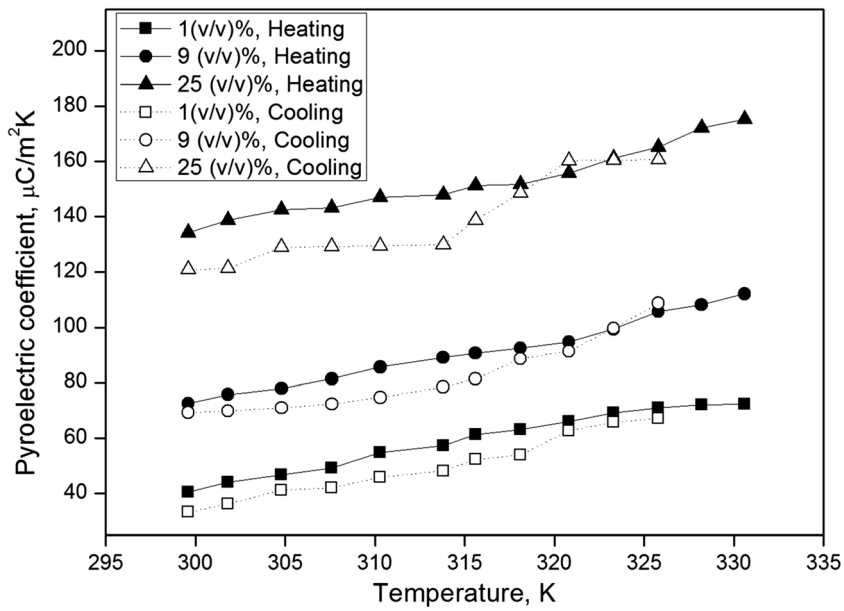

Fig. 8 Variations of pyroelectric coefficient of LN/PVDF nanocomposites with temperature for heating and cooling

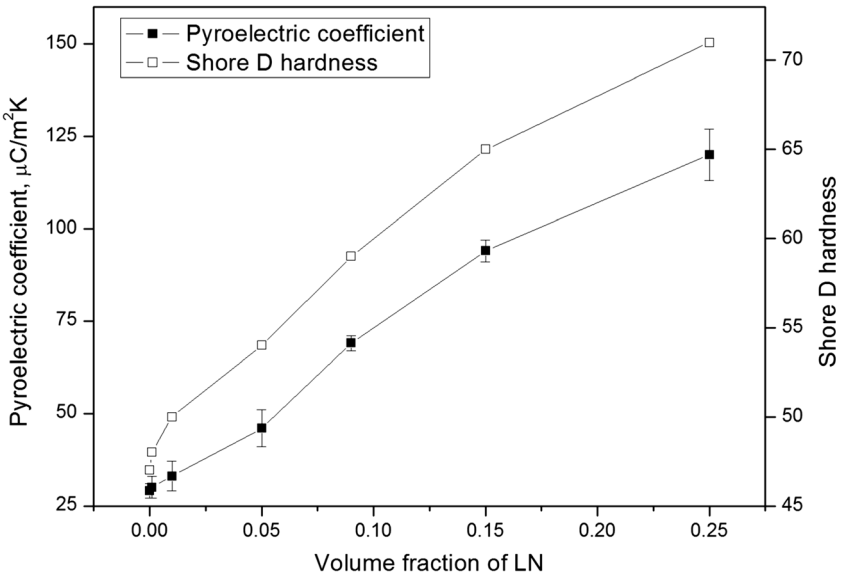

Fig. 9 Variations of pyroelectric coefficient (cooling cycle) and Shore D hardness of LN/PVDF nanocomposites with volume fractions of LN

variations in dielectric loss are from 0.034 to 0.318. The reported value of dielectric constant for pure PVDF film is 11 at 1 kHz [13]; in our measurements it is 10.19, which is rather close to the reported value. It is found that both dielectric constant and loss decrease as frequency increases, but above 1 MHz the dielectric constant and above 100 kHz the dielectric loss show a slight increase. It can also be noticed that the dielectric constant decreases sharply as the frequency increases for higher filler concentrations, but in the high frequency region, the decrease is much less. More or less similar variation occurs for dielectric loss as well.

The increase in dielectric constant with increase in LN content can be attributed to an enhancement in internal polarization of the samples. At lower frequencies (say, below 1 kHz) the dielectric constants of the nanocomposites are higher than the expected values for higher filler concentrations. So it is clear that there must be other contributions to polarization, which enhance the dielectric constant at low frequencies. The observed extra polarization might be from space charge effects [37, 38].

The quantity of accumulated charges depends on the polarity of the polymer. When LN nanoparticles are added to PVDF, the polarization of the composites increase compared to PVDF due to the dipolar contribution from LN. Enhancement in pyroelectric coefficient is obtained for the composite films after poling. Pyroelectric coefficients for all the samples (having area 1 cm^2 and thickness ranging from 55 to 80 μm) were measured and verified on heating as well as cooling (Fig. 8). During heating, in addition to the pyroelectric current, a small current due to the release of trapped space charges will be present. But in the case of cooling the presence of depolarization currents can be eliminated. Figure 9 shows the

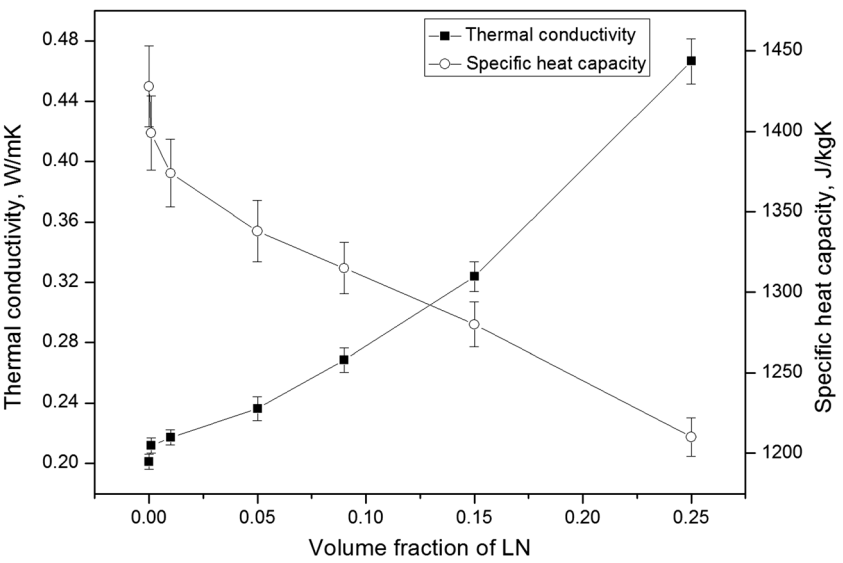

Fig. 10 Variations of thermal conductivity and specific heat capacity of LN/PVDF nanocomposites with volume fractions of LN

Table 1 Variations of pyroelectric figures of merit for IR detection for LN/PVDF nanocomposites with varying volume fractions of LN nanoparticles

Volume fraction of LN/PVDF film	Pyroelectric figures of merit		
	F_I ($\times 10^{-3}$ μCm/J)	F_V ($\times 10^{-3}$ μCm/J)	F_D ($\times 10^{-3}$ μCm/J)
0.00	21.71	2.13	117.74
0.001	23.59	2.29	116.50
0.01	26.93	2.55	120.43
0.05	38.12	3.40	127.07
0.09	53.99	4.45	143.27
0.15	76.56	5.76	153.42
0.25	104.96	6.76	186.13

variation of pyroelectric coefficients during cooling for varying volume fractions of LN/PVDF nanocomposites. It is found that the average value of pyroelectric coefficient increases from 31 $\mu Cm^{-2} K^{-1}$ to 127 $\mu Cm^{-2} K^{-1}$ as the LN concentration in the PVDF matrix increase from volume fraction 0 to 0.25. At higher volume fractions of LN, the pyroelectric coefficient increases because of the presence of a higher proportion of pyroelectric material and increased likelihood of ceramic paths connecting the upper and lower electrodes of the sample.

It is found that thermal conductivity of the nanocomposites increase from 0.2 $Wm^{-1} K^{-1}$ to 0.47 $Wm^{-1} K^{-1}$ with increase in filler concentration, whereas the specific heat capacity decreases from 1428 $Jkg^{-1} K^{-1}$ to 1210 $Jkg^{-1} K^{-1}$. The variations of thermal conductivity and specific heat capacity with filler concentration are shown in Fig. 10.

The important properties to look for in a thermal/infrared sensor material are, low dielectric constant and loss, high pyroelectric coefficient, low specific heat capacity and thermal conductivity. The important figures of merit for infrared pyroelectric detector materials are [39–42],

$$F_I = \frac{p(T)}{C} \tag{2}$$

$$F_V = \frac{p(T)}{C\varepsilon} \tag{3}$$

$$F_D = \frac{p(T)}{C\sqrt{\varepsilon'}} \tag{4}$$

where F_I, F_V, F_D and ε' are the figures of merit for high current sensitivity, high voltage responsivity and high detectivity respectively. These have been calculated for each of the LN/PVDF nanocomposites and in the calculations the values of the dielectric constant and dielectric loss at 1 kHz were used. It is found that the figures of merit increase with increase of filler concentration. Variations of the above figures of merit for varying volume fractions of LN are tabulated in Table 1. These figures of merit have been compared with the corresponding values reported in literature on other comparable composites [43]. It is found that F_I, F_V and F_D for the present LN/PVDF nanocomposites are higher than the values reported earlier for different composites of this class, made by dispersing polycrystalline ceramic particles in polymer matrix

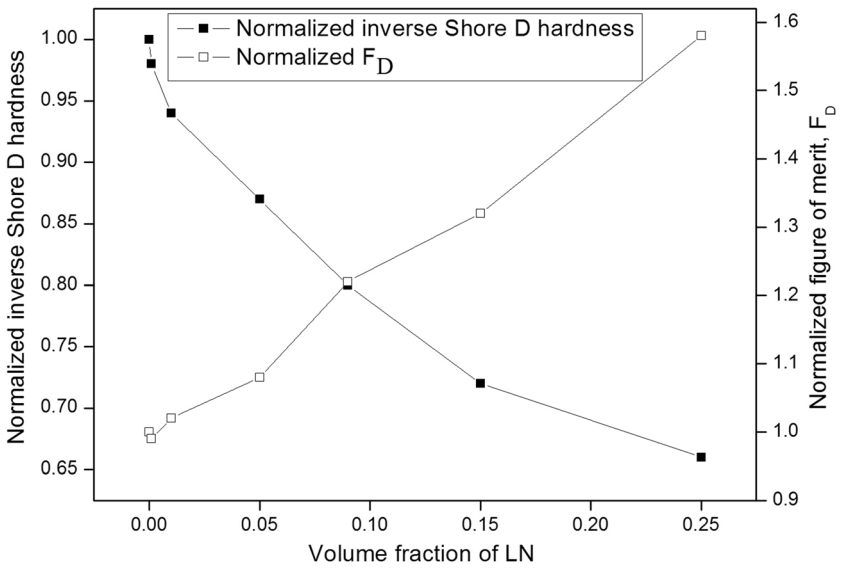

Fig. 11 Variations of normalized pyroelectric figure of merit F_D and normalized inverse Shore D hardness for LN/PVDF nanocomposites with volume fractions of LN

[44–49]. These are also higher than the values reported for pure PVDF and pure P(VDF-TrFE) (Poly (vinylidene fluoride- trifluoro ethylene)) [43]. It is found that LT/PVDF nanocomposites, where LT stands for Lithium tantalate, exhibit higher figures of merit than the present LN/PVDF nanocomposites [50]. Since different authors have followed different definitions for pyroelectric figures of merit and the concentrations of ceramics in the composite taken differently, a direct comparison of the values in the form of a table is found difficult.

Variation of the figure of merit for high detectivity, (F_D), normalized to the corresponding value for pure PVDF, plotted against volume fractions of LN nanopowder, are shown in Fig. 11. It can be seen that the figure of merit increases more or less linearly with filler concentration, which is in tune with mean field approximation [51].

Filler materials in the form of powders or fibres can be added to thermoplastic fluropolymers like PVDF to accomplish improvement in specific properties like strength, stiffness, lubricity etc. Hardness of polymers (rubbers, plastics) is usually measured by the Shore scales. The Shore A scale is used for 'softer' rubbers while the Shore D scale is for 'harder' elastomers/thermoplastics. Shore hardness is often used as a proxy to flexibility for the specification of elastomers/plastics. For LN/PVDF nanocomposite films, it is found that the Shore D hardness increases with increasing volume fractions of LN nanopowder in the composite, as shown in Fig. 9. The variation of inverse Shore D hardness, normalized to the value for pure PVDF, with varying volume fractions of LN is also shown in Fig. 11. Since Shore hardness scales inversely with the flexibility of the polymer, one can notice that the samples get harder as the LN concentration in the composite increases.

From Fig. 11 it is clear that the pyroelectric figure of merit compete with Shore hardness or flexibility of the composite. Depending on the application, the Shore hardness of the composite shall be fixed, which automatically fixes the figure of merit or thermal/infrared detection sensitivity of the material. In the case of other figures of merit, F_I and F_V, similar variations were obtained. Also it can be noticed that at the volume fraction of about 0.10, where the Shore hardness curve meets the figures of merit curve, the LN/PVDF nanocomposite possesses good flexibility as well as good figure of merit for high current sensitivity (F_I), high voltage responsivity (F_V) and high detectivity (F_D). So we can conclude that the volume fraction 0.10 of LN provides the best composition for sensing application, providing good flexibility simultaneously. So by preparing the filler particles in the nanometer scales, we have been able to obtain simultaneously good pyroelectric detection sensitivity along with high flexibility for this composite.

Conclusions

The pyroelectric coefficients and figures of merit for LN/PVDF nanocomposite films with variable volume fractions have been reported for the first time. LN nanopowders are prepared following a novel technique. We have reported the thermal conductivity, specific heat capacity, dielectric constant, dielectric loss and Shore D hardness of these nanocomposites. It is found that pyroelectric coefficient, dielectric constant and thermal conductivity increase significantly with filler loading, while specific heat capacity decreases. All the three relevant pyroelectric figures of merit have been evaluated from these parameters for their possible use as pyroelectric thermal/infrared detectors. A comparison of these with corresponding Shore hardness for these materials shows that improvement in pyroelectric figure of merit is at the expense of the flexibility of the sensor material. All these properties are compared with those of pure β-PVDF film, which is commercially available currently for the same application.

Acknowledgments Work supported by DST, Government of India under Nanomission scheme (SR/NM/NS-30/2010). One of the authors (MSJ) thanks DST, New Delhi for a fellowship under PURSE scheme. Sophisticated Analytical Instrument Facility (SAIF), STIC, Cochin is gratefully acknowledged for sample characterization and technical support.

References

1. Lee J, Mahendra S, Alvarez PJJ (2010) Nanomaterials in the construction industry: a review of their applications and environmental health and safety considerations. ACS Nano 4:3580–3590
2. Saji VS, Choe HC, Yeung KWK (2010) Nanotechnology in biomedical applications: a review. Int J Nano Biomater 3:119–139
3. Chen X, Xu S, Yao N, Shi Y (2010) 1.6 V nanogenerator for mechanical energy harvesting using PZT nanofibers. Nano Lett 10: 2133–2137
4. Iavicoli I, Fontana L, Leso V, Bergamaschi A (2013) The effects of nanomaterials as endocrine disruptors. Int J Mol Sci 14:16732–16801
5. Huang X, Li L, Liu T, Hao N, Liu H, Chen D, Tang F (2011) The shape effect of mesoporous silica nanoparticles on biodistribution, clearance, and biocompatibility in Vivo. ACS Nano 5:5390–5399
6. Sethi M, Pacardo DB, Knecht MR (2010) Biological surface effects of metallic nanomaterials for applications in assembly and catalysis. Langmuir 26:15121–15134
7. Orvatinia M, Heydarianasl M (2012) A new method for detection of continuous infrared radiation by pyroelectric detectors. Sensors Actuators A Phys 174:52–57
8. Batra AK, Aggarwal MD (2013) Pyroelectric materials: Infrared detectors, particle accelerators, and energy harvesters. SPIE Press Book, ISBN: 9780819493316
9. Rogalski A (2011) Infrared detectors, 2nd edn. CRC Press, Taylor & Francis Group, USA
10. Goniakowski J, Finocchi F, Noguera C (2008) Polarity of oxide surfaces and nanostructures. Rep Prog Phys 71:016501/1-55
11. Rosenman G, Shur D, Krasik YE, Dunaevsky A (2000) Electron emission from ferroelectrics. J Appl Phys 88:6109–6161

12. Lang SB (2005) Pyroelectricity: from ancient curiosity to modern imaging tool. Phys Today 58:31–36
13. Whatmore RW (1986) Pyroelectric devices and materials. Rep Prog Phys 49:1335–1386
14. Muralt P (2001) Micromachined infrared detectors based on pyroelectric thin films. Rep Prog Phys 64:1339–1388
15. Corsi C (2012) Infrared: a key technology for security systems. Adv Opt Technol 2012:838752/1-15
16. Cilulko J, Janiszewski P, Bogdaszewski M, Szczygielska E (2013) Infrared thermal imaging in studies of wild animals. Eur J Wildl Res 59:17–23
17. Kad RS (2013) IR thermography is a condition monitor technique in industry. IJAREEIE 2:988–993
18. Suriani MJ, Ali A, Khalina A, Sapuan SM, Haftirman AS (2012) Detection of defects in natural composite materials using thermal imaging technique. Mater Test 54:340–346
19. Hanemann T, Szabo DV (2010) Polymer-nanoparticle composites: from synthesis to modern applications. Materials 3:3468–3517
20. Graca MPF, Prezas PR, Costa MM, Valente MA (2012) Structural and dielectric characterization of $LiNbO_3$ nano-size powders obtained by Pechini method. J Sol-Gel Sci Technol 64:78–85
21. Rabiei P, Gunter P (2004) Optical and electro-optical properties of submicrometer lithium niobate slab waveguides prepared by crystal ion slicing and wafer bonding. Appl Phys Lett 85:4603–4605
22. Peng Q, Cohen RE (2011) Origin of pyroelectricity in $LiNbO_3$. Phys Rev B 83:220103/1-4
23. Jaffe B, Cook WR Jr, Jaffe H (2012) Piezoelectric ceramics. Academic, London
24. Mohimi A, Richardson P, Catton P, Gan TH, Balachandran W, Selcuk C (2013) High temperature dielectric, elastic and piezoelectric coefficients of shear type lithium niobate crystals. Key Eng Mater 543: 117–120
25. Bhatti IN, Banerjee M, Bhatti IN (2013) Effect of annealing and time of crystallization on structural and optical properties of PVDF thin film using acetone as solvent. IOSR-JAP 4:42–47
26. Satapathy S, Pawar S, Gupta PK, Varma KBR (2011) Effect of annealing on phase transition in poly(vinylidene fluoride) films prepared using polar solvent. Bull Mater Sci 34:727–733
27. Seminara L, Capurro M, Cirillo P, Cannata G, Valle M (2011) Electro-mechanical characterization of piezoelectric PVDF polymer films for tactile sensors in robotics applications. Sensors Actuators A Phys 169:49–58
28. Graz I, Krause M, Gogonea SB, Bauer S, Lacour SP, Ploss B, Zirkl M, Stadlober B, Wagner S (2009) Flexible active-matrix cells with selectively poled bifunctional polymer-ceramic nanocomposite for pressure and temperature sensing skin. J Appl Phys 106:034503/1-5
29. Jeon J, Lee HBR, Bao Z (2013) Flexible wireless temperature sensors based on Ni microparticle filled binary polymer composites. Adv Mater 25:850–855
30. Sanchez-Garcia MD, Gimenez E, Lagaron JM (2008) Morphology and barrier properties of solvent cast composites of thermoplastic biopolymers and purified cellulose fibers. Carbohydr Polym 71: 235–244
31. Byer RL, Roundy CB (1972) Pyroelectric coefficient direct measurement technique and application to a nanosecond-response-time detector. Ferroelectrics 3:333–338
32. Marshall JM, Zhang Q, Whatmore RW (2008) Corona poling of highly (001)/(100)-oriented lead zirconate titanate thin films. Thin Solid Films 516:4679–4684
33. Yun S, Kim JH, Li Y, Kim J (2008) Alignment of cellulose chains of regenerated cellulose by corona poling and its piezoelectricity. J Appl Phys 103:083301/1-4
34. Menon CP, Philip J (2000) Simultaneous determination of thermal conductivity and heat capacity near solid state phase transitions by a photopyroelectric technique. Meas Sci Technol 11:1744–1749
35. Lee SH, Cho HH (2010) Crystal structure and thermal properties of poly(vinylidene fluoride)-carbon fiber composite films with various drawing temperatures and speeds. Fibers Polym 11:1146–1151
36. Yu L, Cebe P (2009) Crystal polymorphism in electrospun composite nanofibers of poly (vinylidene fluoride) with nanoclay. Polymer 50: 2133–2141
37. Murugaraj P, Mainwaring D, Mora-Huertas N (2005) Dielectric enhancement in polymer-nanoparticle composites through interphase polarizability. J Appl Phys 98:054304/1-6
38. Sakai H, Konno K, Murata H (2009) Tuning of threshold voltage of organic field-effect transistors by space charge polarization. Appl Phys Lett 94:073304/1-3
39. Sidney BL, Das-Gupta DK (2000) Pyroelectricity: fundamentals and applications. Ferroelectr Rev 2:217–223
40. Whatmore RW, Watton R (2001) Pyroelectric materials and devices' in 'infrared detectors and emitters: materials and devices'. Kluwer Academic Publishers, The Netherlands
41. Guggilla P, Batra AK, Currie JR, Aggarwal MD, Alim MA, Lal RB (2006) Pyroelectric ceramics for infrared detection applications. Mater Lett 60:1937–1942
42. Rogalski A (2003) Review- infrared detectors: status and trends. Prog Quantum Electron 27:59–210
43. Aggarwal M, Currie JR Jr, Penn BG, Batra AK, Lal RB (2007) Polymer-ceramic composite materials for pyroelectric infrared detectors: an overview. http://ntrs.nasa.gov/archive/nasa/casi.ntrs.nasa.gov/20080013166.pdf
44. Chan HLW, Chan WK, Zhang Y, Choy CL (1998) Pyroelectric and piezoelectric properties of lead titanate/polyvinylidene fluoride-trifluoroethelene 0–3 composites. IEEE Trans Dielectr Electr Insul 5:505–512
45. Zhang QQ, Bernd Ploss HL, Chan W, Choi CL (2000) Integrated pyroelectric arrays based on PCLT/P(VDF-TrFE) composite. Sensors Actuators A Phys 86:216–219
46. Hilczer B, Kulek J, Markiewicz E, Kosec M (2003) Dielectric and pyroelectric response of PLZT-P(VDF/TrFE) nano-composites. Ferroelectrics 293:253–265
47. Guggilla P, Batra AK, Edwards ME (2009) Electrical characterization of LiTaO3:P(VDF–TrFE) composites. J Mater Sci 44:5469–5474
48. Navid A, Lynch CS, Pilon L (2010) Purified and porous poly(vinylidene fluoride-trifluoroethylene) thin films for pyroelectric infrared sensing and energy harvesting. Smart Mater Struct 19: 055006/1-13
49. Dietze M, Krause J, Solterbeck CH, Es SM (2007) Thick film polymer-ceramic composites for pyroelectric applications. J Appl Phys 101:054113/1-7
50. Jayalakshmy MS, Philip J (2014) Pyroelectric figures of merit and associated properties of LiTaO3/polyvinylidene difluoride nanocomposites for thermal/infrared sensing. Sensors Actuators A Phys 206: 121–126
51. Barber P, Balasubramanian S, Anguchami Y, Gong S, Wibowo A, Gao H, Ploehn HJ, Loye HCZ (2009) Polymer composite and nanocomposite dielectric materials for pulse power energy storage. Materials 2:1697–1733